1st Konstantinos Fragkos
Resilient Society Department
Eratosthenes Centre of Excellence
Limassol, Cyprus
kostas.fragkos@eratosthenes.org.cy

2nd Georgia Charalampous
Resilient Society Department
Eratosthenes Center of Excellence
Limassol, Cyprus
Department of Civil Engineering & Geomatics
Cyprus University of Technology
Limassol, Cyprus
georgia.charalambous@eratosthenes.org.cy

3rd Ilias Fountoulakis
Institute for Astronomy, Astrophysics, Space Applications and Remote Sensing
National Observatory of Athens Athens, Greece
Research Centre for Atmospheric Physics and Climatology
Academy of Athens Athens, Greece
ifountoulakis@Academyofathens.gr

4th Kyriakoula Papachristopoulou
Institute for Astronomy, Astrophysics, Space Applications and Remote Sensing
National Observatory of Athens
Athens, Greece
kpapachr@geol.uoa.gr

5th Diofantos Hadjimitsis
Resilient Society Department
Eratosthenes Center of Excellence
Limassol, Cyprus
Department of Civil Engineering & Geomatics
Cyprus University of Technology
Limassol, Cyprus
d.hadjimitsis@cut.ac.cy

6th Stelios Kazadzis
Physikalisch-Meteorologisches Observatorium Davos
World Radiation Center
Davos, Switzerland
Stelios.Kazadzis@pmodwrc.ch

Next-Day Solar Irradiance Forecasting: A Preliminary Study in Limassol

Abstract—This study presents a preliminary evaluation of a next-day solar irradiance forecast system in Limassol, Cyprus, over six months. For the evaluation, forecasted Global Horizontal Irradiance (GHI) was compared with high-quality ground measurements. The system showed strong correlation with measured values at both hourly and daily timescales. Hourly forecasts exhibited a correlation coefficient (r^2) of 0.84 and a Mean Bias Error (MBE) of 23.4 W/m² (4.8%), while daily energy forecasts showed improved performance with an r^2 of 0.86 and an MBE of 0.3 kWh/m² (4.7%). The Root Mean Squared Error (RMSE) was 123.7 W/m² (25.4%) for hourly forecasts and 0.8 kWh/m² (13%) for daily forecasts, indicating that daily aggregation reduces error magnitudes by averaging out short-term fluctuations and discrepancies. Some discrepancies were due to the model's limited ability to capture cloud and aerosol variations. Future work will focus on investigating these factors to enhance the forecast system's accuracy and reliability.

Index Terms—Solar Irradiance Forecasting, Next-Day Energy Forecast, Cloud Modification Factor, Aerosol Load

I. Introduction

Solar energy is the most abundant renewable energy source available in nature. Its proper utilization has the potential to significantly mitigate major environmental issues, such as reducing greenhouse gas emissions that contribute to global warming. Despite its benefits, harnessing solar energy presents several challenges that currently prevent its full utilization [1].

979-8-3503-7592-3/24/$31.00 © 2024 IEEE

These challenges include grid integration [2], accurate cost analysis [3], and variability in solar energy supply due to weather and other environmental factors [4], among others.

One of the key aspects in addressing these challenges is the accurate forecasting of solar irradiance. Solar irradiance forecasting is critical for the effective planning and operation of solar energy systems [5]. It enables better grid integration, optimizes energy production, and aids in cost-effective management of solar resources [6] [7]. Forecasting can be categorized into different time-scales, each serving specific purposes:

- Nowcasting: Provides short-term forecasts, typically up to a few hours ahead, and is essential for real-time energy management and grid stability.
- Short-term forecasting: Covers the next few hours to a day and is crucial for daily operation and scheduling of solar power plants.
- Medium-term forecasting: Ranges from a few days to a week and supports operational planning and maintenance scheduling.
- Long-term forecasting: Includes seasonal forecasts and beyond, which are vital for strategic planning, investment decisions, and policy-making.

In this context, next-day solar irradiance forecasting holds particular importance. Accurate next-day forecasts are essential for day-ahead market operations, energy trading, and efficient scheduling of solar power generation [8] [9]. These forecasts help in balancing supply and demand, minimizing the need for backup power, and reducing operational costs [9].

The scope of the current study is to evaluate the accuracy of a next-day solar irradiance forecast system in Limassol, Cyprus by comparing them with actual measurements obtained from a high-quality pyranometer. This preliminary evaluation aims to quantify the forecast performance against measurements using key metrics such as Mean Absolute Error (MAE), Root Mean Squared Error (RMSE), and Mean Bias Error (MBE). The structure of the paper is as follows: Section II outlines the methodology for solar irradiance forecasting and describes the tools employed for evaluation against real-world measurements. Section III presents the results, and Section IV concludes with a summary of the key findings.

II. Methodology and Data

A. Solar irradiance forecast

The next day irradiance forecast over Limassol is performed in a two-step procedure. Initially, the clear sky surface solar irradiance at horizontal level (GHI) is calculated for each hour, precalculated look-up tables (LUT) derived from radiative transfer model (RTM) simulations and forecasted quantities of physical parameters (aerosol properties, total ozone column, total water vapor) that affect GHI under cloudless conditions. The second step includes the calculation of the cloud modification factor (CMF) derived from the Weather Research and Forecasting (WRF). Finally, the clear sky GHI is multiplied with the CMF to derive the final forecast.

TABLE I
INPUT PARAMETERS FOR CREATING THE LUT USING LIBRADTRAN

Parameter	Range/Step
SZA	1-89°/1°
AOD550	0-2/0.05, 2.5 and 3
SSA550	0.6-1/0.1
AE	0-2/0.4
TCWV	0.5-3 cm/0.5 cm
TOC	200-500 DU/100 DU

Here is a rephrased version of your text that aims to reduce similarity while retaining the original meaning and technical accuracy:

The Look-Up Table (LUT) was developed to include Global Horizontal Irradiance (GHI) values simulated using the LibRadtran radiative transfer model (RTM) [10]. These simulations accounted for varying Solar Zenith Angles (SZAs) and an extensive range of atmospheric parameters influencing GHI under cloudless conditions. The radiative transfer solver, sdisort [11], was employed to carry out pseudospectral simulations at a spectral resolution of 1 nm, spanning the wavelength range of 280–3000 nm. These calculations incorporated the LOWTRAN band model parameterization [12], as adapted from the SBDART algorithm [13], to represent molecular absorption processes. The extraterrestrial solar spectrum, as described by Kurucz [14], with a resolution of 1.0 nm, and the US standard atmospheric profile [15], served as reference inputs for these simulations. The surface albedo was consistently set to 0.2. GHI values for clear-sky conditions were subsequently simulated for all possible parameter combinations outlined in Table I.

The clear-sky GHI estimates are calculated by linear interpolation in the six dimensions (6D) of the precalculated GHI LUT using the corresponding inputs. Specifically, the solar zenith angle (SZA) is calculated for each hour from sunrise to sunset. The main input parameters for the clear-sky computations are the forecasted AOD at 550 nm (AOD550) and the total water vapor (TWV) from CAMS. Other aerosol parameters obtained from CAMS include the single scattering albedo at 550 nm and the Angstr˚ om exponent (AE). The¨ forecasts for the day of interest are values from the Copernicus Atmosphere Monitoring Service (CAMS) global atmospheric composition forecasts [16] [17] with a spatial resolution of 40 km. Finally, the total ozone column (TOC) is obtained from the Tropospheric Emission Monitoring Internet Service (TEMIS) using the GOME-2 Assimilated Ozone Fields (METOP-B), providing a forecast of the total ozone column (TOC) at a spatial resolution of 1x1 degree [18]. To account for the fact that the RTM simulations are based on the average EarthSun distance, a postprocessing adjustment is applied to the clear-sky GHI values in the LUT. This correction ensures that the values are accurate for the actual Earth–Sun distance corresponding to the specific day of the year.

Cloud Modification Factors, defined as the ratio between the all-sky and clear-sky surface solar radiation from the WRF, are derived every 1 hour from the model, with a resolution of 2x2 km.

B. Data

GHI measurements were obtained from an EKO Instruments MS-80 pyranometer, located at the Eratosthenes solar radiation station [19] situated at coordinates 34.67°N, 33.04°E, and 26 meters above sea level. The station was established in December 2023. The MS-80 is a secondary standard pyranometer as per ISO 9060:2018, featuring a fast-response thermopile with a 95% response time within 0.5 seconds, a nonlinearity of less than 0.2%, and an expanded calibration uncertainty (2σ) of ±0.56%. The instrument sensitivity is 11.34 μV W^{-1} m^{-2}. The pyranometer data were sampled every second, with
1-minute averages recorded using a Campbell Scientific CR1000X datalogger. To identify cloudless conditions, images from an EKO-MS ASI-16 all-sky imager installed at the same

location were utilized. These images were captured at a resolution of 1 minute.

III. Results

Fig.1 shows the time series of the daily insolation, illustrating the daily energy levels in kWh/m², for the period December 2023 to July 2024, calculated from the forecasts and the actual measurements. Note that for consistency reasons in the computation of the daily solar energy integrals from the measurements, only the instantaneous values at each hour, the same as the forecasts, were used.

The measured insolation values exhibit more variability compared to the forecasted values, which tend to be smoother. This variability is likely due to transient weather conditions, such as cloud cover that are captured by the measurements and diurnal variations in aerosol load that might not be fully accounted for in the forecast model. However, the overall consistency between the forecasted and measured data demonstrates the robustness of the forecasting approach in capturing daily insolation patterns. In the next paragraph a more quantitative evaluation of the

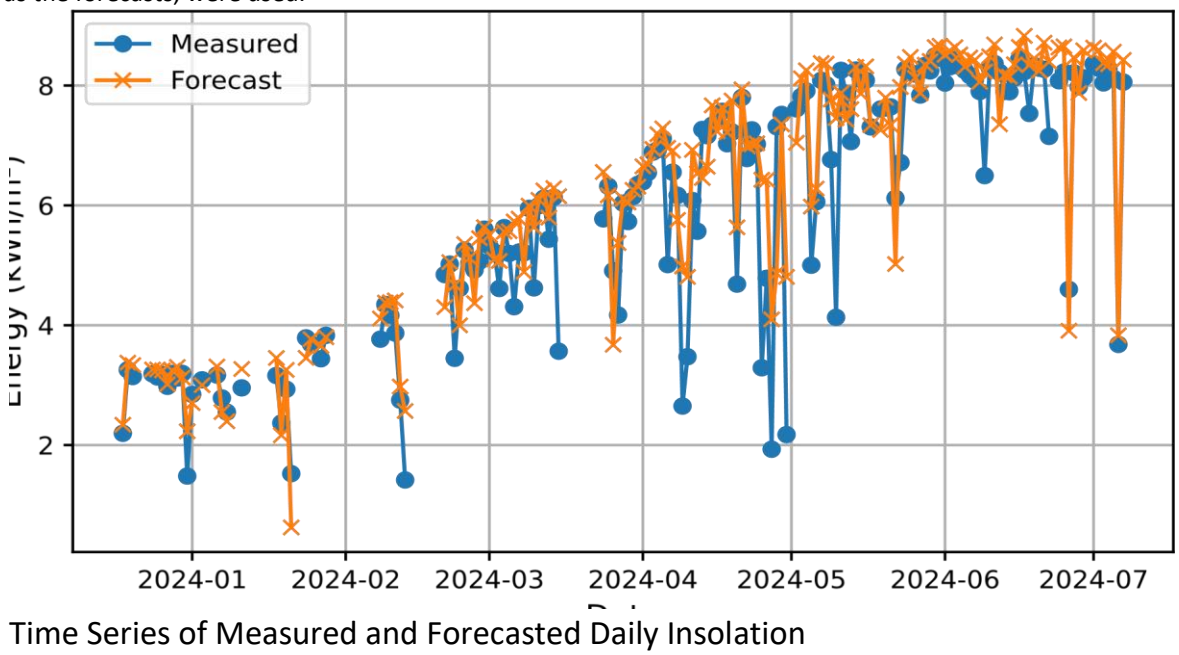

Fig. 1. Time Series of Measured (blue circles) and Forecasted (orange crosses) Daily Insolation over Limassol, for the period 12/2023 - 07/2024.

There is a clear seasonal trend observed in both the measured and forecasted insolation values. As expected, the daily insolation increases towards the summer months, with peak values occurring around June and July. The highest measured daily insolation reaches approximately 8.5 kWh/m² on 30 May 2024 (8.5 kWh/m² from the forecast), while the minimum of approximately 1.4 kWh/m² (2.6 kWh/m² from the forecast) was observed on 13 February 2024.

The forecasted values generally follow the trend of the measured values closely, indicating a reasonable level of accuracy in the next-day solar irradiance forecasts. There are instances where the forecasted values slightly overestimate or underestimate the measured values. This discrepancy could be attributed to the inherent variability in weather conditions and the limitations of the forecasting model to account for the actual aerosol loading conditions. During summer months in Limassol, the attenuation of solar irradiance from aerosols can be as significant as that from clouds [20].

forecast model is performed.

A. Evaluation of the hourly irradiance forecast

Fig. 2 presents the overall performance of the forecasted system at the (instantaneous) 1-hour timescale by comparing the forecasted GHI values against ground-based measurements. The scatter plot (Fig 2a) highlights a strong correlation ($r^2 = 0.84$) between forecasted and measured GHI values, demonstrating the forecasting model's accuracy. The red dashed line represents perfect correlation (y = x), and the clustering of data points around this line indicates a high level of agreement between forecasts and actual measurements. Points above the line of perfect correlation show a tendency for the model to overestimate GHI values, particularly evident in lower irradiance ranges (less than 500 W/m²). This suggests that the forecasting system performs differently across various irradiance levels. Overestimations are more pronounced at lower irradiance levels, possibly due to challenges in accurately predicting cloud cover or aerosol load. During periods with

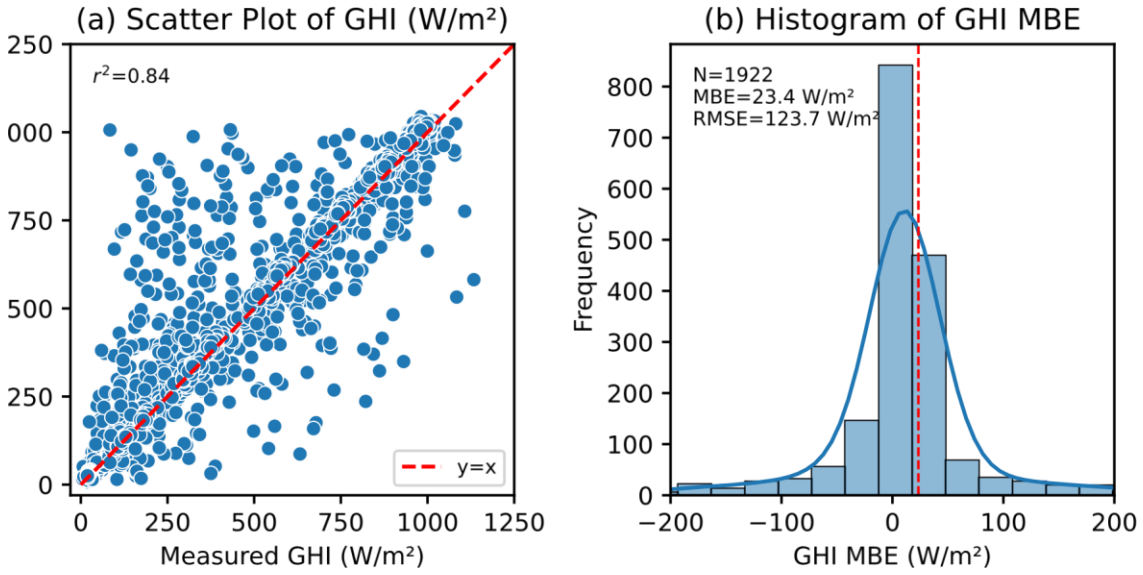

Fig. 2. (a) Comparison between forecasted and measured GHI)for all hourly values. (b) Frequency distribution of the GHI MBE

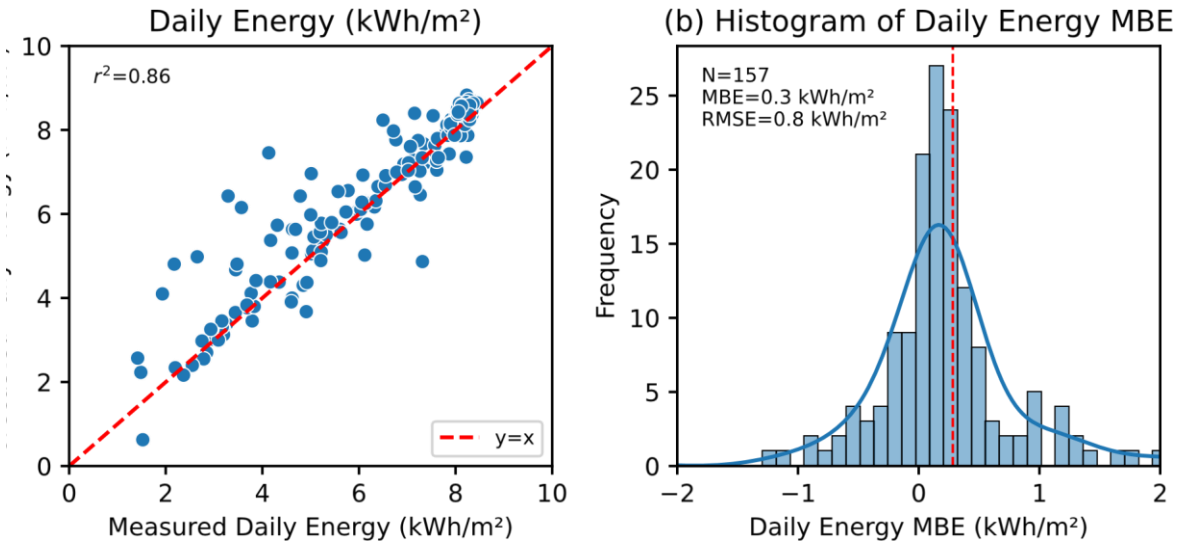

(a) Scatter Plot of

Fig. 3. (a) Comparison of the forecasted versus measured daily energy. (b) Frequency distribution of the daily energy MBE

higher irradiance levels (above 500 W/m²), the forecasts tend to align more closely with actual measurements, reflecting the model's capability to accurately predict clear sky conditions. The histogram (Fig. 2b) displays the distribution of the Mean Bias Error (MBE) for forecasted GHI values. The majority of errors are centered around the mean MBE of 23.4 W/m² (4.8%), with most values falling within the range of -200 to 200 W/m². This concentration of errors around the mean suggests that the model's overestimations are consistent but not excessively large, contributing to the overall reliability of the forecasts. The RMSE of 123.7 W/m² (25.4%) reflects the average magnitude of the forecast errors, combining both the bias and variability of the errors. Additionally, 76% of the forecasted values fall within a margin of ±50 W/m² from the measured values. This fact underscores the model's high accuracy and reliability for most cases.

B. Evaluation of the daily energy forecast

The daily insolation is calculated from the integration of the hourly GHI forecasts and measurements as discussed above. Fig. 3 evaluates the performance of the forecasted system on

a daily scale through a comparison of the predicted daily energy values against ground-based measurements. Daily forecasts show a higher correlation (Fig. 3a; r^2 =0.86) with measured values compared to hourly forecasts (r^2 = 0.84). Aggregating hourly data into daily totals averages out shortterm fluctuations and errors, resulting in a smoother and more accurate representation of daily energy. The forecasted values align closely with the measured values, except for some scatter, particularly at the lower energy levels.

The MBE (Fig. 3b) for daily energy forecasts is 0.3 kWh/m² (4.7%), slightly lower than the MBE for hourly forecasts (4.8%). This indicates that the model's tendency to overestimate remains on a daily scale. However, the RMSE for daily energy forecasts is 0.8 kWh/m² (13%), compared to 25.4% for hourly forecasts. The lower RMSE for daily forecasts suggests that daily aggregation reduces the overall error magnitude, smoothing out discrepancies observed in shorter timescales (e.g., transient clouds that are not captured by the model).

The evaluation of the daily energy forecast system reveals robust performance with a high correlation and reduced bias compared to hourly forecasts. Aggregating hourly values into daily totals averages out short-term fluctuations, resulting in more accurate and reliable daily energy forecasts.

IV. Conclusions

A preliminary evaluation of the next-day irradiance forecast system in Limassol has been conducted over a 6-month period. The system's performance on an hourly basis, as assessed by comparison with high-quality GHI measurements, was very good, with further improvements observed at the daily energy level. The hourly forecasts showed a strong correlation with measured values (r^2 = 0.84), while the daily energy forecasts demonstrated even higher accuracy (r^2 = 0.86). The MBE was 23.4 W/m² (4.8%) for hourly forecasts and 0.3 kWh/m² (4.7%) for daily forecasts, indicating a slight overestimation tendency. The RMSE was 123.7 W/m² (25.4%) for hourly forecasts and 0.8 kWh/m² (13%) for daily forecasts, highlighting the effectiveness of daily aggregation in reducing error magnitudes.

Some discrepancies could mainly be attributed to the model's potential shortcomings in fully capturing cloud conditions, as well as differences between forecasted and actual aerosol load. These discrepancies were more pronounced at lower irradiance levels, suggesting that the model could benefit from improved cloud cover and aerosol load forecasting. The high correlation and reduced bias at the daily level demonstrate the robustness of the forecasting system and its potential for reliable solar energy management.

Future work will focus on deeper investigation into the causes of forecast discrepancies, particularly the impacts of cloud conditions and aerosol loading. Additionally, extending the evaluation period and including more diverse climatic conditions could provide a more comprehensive assessment of the forecast system's performance.

Acknowledgment

The authors acknowledge the 'EXCELSIOR': ERATOSTHENES: Excellence Research Centre for Earth Surveillance and Space-Based Monitoring of the Environment H2020 Widespread Teaming project (www.excelsior2020.eu). The 'EXCELSIOR' project has received funding from the European Union's Horizon 2020 research and innovation programme under Grant Agreement No. 857510, from the Government of the Republic of Cyprus through the Directorate General for the European Programmes, Coordination and Development and the Cyprus University of Technology.

References

[1] O. A. Al-Shahri et al., 'Solar photovoltaic energy optimization methods, challenges and issues: A comprehensive review', Journal of Cleaner Production, vol. 284, p. 125465, 2021.

[2] M. Shafiullah, S. D. Ahmed, and F. A. Al-Sulaiman, 'Grid Integration Challenges and Solution Strategies for Solar PV Systems: A Review', IEEE Access, vol. 10, pp. 52233–52257, 2022.

[3] J. Heeter, A. Sekar, E. Fekete, M. Shah, and J.J. Cook, 'Affordable and Accessible Solar for All: Barriers, Solutions, and OnSite Adoption Potential', No. NREL/TP-6A20-80532, National Renewable Energy Lab.(NREL), Golden, CO, United States, 2021. https://doi.org/10.2172/1820098.

[4] M. M. Hasan et al., 'Harnessing Solar Power: A Review of Photovoltaic Innovations, Solar Thermal Systems, and the Dawn of Energy Storage Solutions', Energies, vol. 16, no. 18, 2023.

[5] K. Sudharshan, C. Naveen, P. Vishnuram, D. V. S. Krishna Rao Kasagani, and B. Nastasi, 'Systematic Review on Impact of Different Irradiance Forecasting Techniques for Solar Energy Prediction', Energies, vol. 15, no. 17, 2022.

[6] D. Yang et al., 'A review of solar forecasting, its dependence on atmospheric sciences and implications for grid integration: Towards carbon neutrality', Renewable and Sustainable Energy Reviews, vol. 161, p. 112348, 2022.

[7] D. Yang, E. Wu, and J. Kleissl, 'Operational solar forecasting for the real-time market', International Journal of Forecasting, vol. 35, no. 4, pp. 1499–1519, 2019.

[8] Y. Wang, D. Millstein, A. D. Mills, S. Jeong, and A. Ancell, 'The cost of day-ahead solar forecasting errors in the United States', Solar Energy, vol. 231, pp. 846–856, 2022.

[9] M. David, J. Boland, L. Cirocco, P. Lauret, and C. Voyant, 'Value of deterministic day-ahead forecasts of PV generation in PV + Storage operation for the Australian electricity market', Solar Energy, vol. 224, pp. 672–684, 2021.

[10] C. Emde et al., 'The libRadtran software package for radiative transfer calculations (version 2.0.1)', Geoscientific Model Development, vol. 9, no. 5, pp. 1647–1672, 2016.

[11] A. Dahlback and K. Stamnes, 'A new spherical model for computing the radiation field available for photolysis and heating at twilight', Planetary and Space Science, vol. 39, no. 5, pp. 671–683, 1991.

[12] J. H. Pierluissi and G.-S. Peng, 'New Molecular Transmission Band Models For LOWTRAN', Optical Engineering, vol. 24, no. 3, p. 243541, 1985.

[13] R. L. Kurucz, 'Synthetic Infrared Spectra', Symposium - International Astronomical Union, vol. 154, pp. 523–531, 1994.

[14] P. Ricchiazzi, S. Yang, C. Gautier, and D. Sowle, 'SBDART: A Research and Teaching Software Tool for Plane-Parallel Radiative Transfer in the Earth's Atmosphere', Bulletin of the American Meteorological Society, vol. 79, no. 10, pp. 2101–2114, 1998.

[15] R.A. McClatchey, Optical properties of the atmosphere, No. 411, Air Force Cambridge Research Laboratories, Office of Aerospace Research, United States, 1972.

[16] V.-H. Peuch et al., 'The Copernicus Atmosphere Monitoring Service: From Research to Operations', Bulletin of the American Meteorological Society, vol. 103, no. 12, pp. E2650–E2668, 2022.

[17] S. Remy et al., 'Description and evaluation of the tropospheric aerosol´ scheme in the European Centre for Medium-Range Weather Forecasts (ECMWF) Integrated Forecasting System (IFS-AER, cycle 45R1)', Geoscientific Model Development, vol. 12, no. 11, pp. 4627–4659, 2019.

[18] H. J. Eskes, P. F. J. Van Velthoven, P. J. M. Valks, and H. M. Kelder, 'Assimilation of GOME total-ozone satellite observations in a threedimensional tracer-transport model', Quarterly Journal of the Royal Meteorological Society, vol. 129, no. 590, pp. 1663–1681, 2003.

[19] K. Fragkos et al., 'Introducing the Solar Radiation and Energy Laboratory of the Eratosthenes' Centre of Excellence: Overview of Activities', Environmental Sciences Proceedings, vol. 26, no. 1, 2023.

[20] I. Fountoulakis et al., 'Effects of Aerosols and Clouds on the Levels of Surface Solar Radiation and Solar Energy in Cyprus', Remote Sensing, vol. 13, no. 12, 2021.